J. Fluid Mech. (1988), *vol.* 188, *pp.* 253–274
Printed in Great Britain

Separation and reattachment near the leading edge of a thin oscillating airfoil

By TUNCER CEBECI, A. A. KHATTAB AND S. M. SCHIMKE
Aerodynamics Research and Technology, Douglas Aircraft Company, Long Beach, CA 90846, USA

(Received 12 January 1987)

The evolution of unsteady boundary layers in the vicinity of the leading edge of a thin oscillating airfoil has been examined with a novel numerical method which is able to deal with the movement of the stagnation point and with regions of reverse and separated flow. Solutions to the unsteady boundary-layer equations, with a prescribed pressure distribution which causes flow reversal and separation, demonstrate the importance of numerical steps in distance and time and that a requirement similar to the stability criterion of Courant, Friedrichs and Lewy must be satisfied to avoid numerical errors. At the lower reduced frequencies of the investigation, solutions could not be obtained with this procedure and it was necessary to introduce interaction between the viscous and inviscid flows. The solutions obtained with the interactive method were increasingly different from those without interaction as the reduced frequency was decreased towards zero and, for some combinations of Reynolds number and frequency, exhibited behaviour consistent with the instability of separation bubbles.

1. Introduction

The lift and drag characteristics of airfoils at moderate Reynolds numbers can be affected by separation bubbles which occur close to the leading edge and, at high angles of attack, can increase in size to cause stall. The added complexity of unsteady motion such as that associated with the rotor blades of helicopters implies that the flow characteristics are influenced by amplitude and frequency and that, in particular, the stall characteristics can be considerably modified. The investigations of Carr, McAlister & McCroskey (1977), Francis, Keese & Retelle (1983), Daley & Jumper (1984) and Lorber & Covert (1986) examined these effects over limited ranges of the parameters, and that of Carr *et al.* (1977) provides detailed information on the mechanism of dynamic stall of an oscillating airfoil. It appears that stall is associated with flow reversals in the unsteady boundary layer and that these may translate downstream or upstream depending upon various parameters including the radius of the leading edge of the airfoil. At some stage in the cycle, stall occurs and is preceded by a vortex which forms close to the surface and is probably associated with a breakdown of the unsteady boundary layer.

The above physical problems involve laminar, transitional and turbulent flow and their representation requires a numerical calculation procedure that can provide accurate solutions to conservation equations in all regions of flow as well as appropriate transition and turbulence models. Here we are concerned with the numerical solution procedure, its development to represent the regions of reverse flow and its use in examining the nature of solutions for parameters close to those

associated with stall. The emphasis is on regions of flow close to the leading edge of a thin oscillating airfoil and calculations are performed with a prescribed pressure gradient and with interaction between solutions of the viscous and inviscid equations. With the configuration chosen, an analytical solution for the potential-flow equations was available.

Previous consideration of steady boundary layers and their solution by an interactive procedure has been reported by Cebeci, Stewartson & Williams (1981) for a model problem consisting of a thin ellipse at incidence. Their study showed that the solutions were well behaved and unseparated provided the reduced angle of attack was less than 1.155. At higher angles separation occurred with an associated singularity, which was overcome by the use of the interactive procedure, and results were obtained for small regions of separated flow. There is, however, a limiting size of separation bubble beyond which Cebeci *et al.* (1981) could not obtain solutions and this may be related to the physical phenomenon of open separation and stall. A similar result was obtained by Stewartson, Smith & Kaups (1982) who used a triple-deck approach and found that their calculations of separation bubbles could break down with a small increment in pressure gradient. They also observed that their solutions were not unique and their results may imply that large separation bubbles cannot exist in laminar flows at high Reynolds numbers.

The unsteady-flow calculations reported here were obtained with Keller's (1974) box method for the solution of the boundary-layer equations. In regions of flow reversal, a requirement similar to the stability criterion of Courant, Friedrichs & Lewy (CFL), see Isaacson & Keller (1966), is satisfied by the use of the characteristic-box procedure discussed by Keller (1978) and Cebeci (1986), and the interactive procedure is based on the Hilbert integral previously used by Cebeci *et al.* (1981). This combination of methods represents the best possible approach available to the authors and allows the importance of the stability criterion β to be examined as well as the structure of the solutions. Of necessity, a limited number of parameters is considered but they encompass a range of relevance to oscillating airfoils.

The flow configuration under consideration, equations, and initial and boundary conditions are examined in the following section, which is followed by a brief description of the solution procedure. The results are presented and discussed in §4 and the paper ends with a summary of the more important conclusions.

2. Flow configuration, conservation equations, initial and boundary conditions

We consider flow over an ellipse with a thickness ratio $t_1(\equiv b/a)$ much less than unity at an angle of attack α. The body surface is defined by

$$x = -a\cos\theta, \quad y = at_1\sin\theta \quad (-\pi \leqslant \theta \leqslant \pi),$$

and the corresponding external velocity for steady flow can be deduced from inviscid-flow theory to be

$$\overline{u_e^0}(s,t) = \frac{\xi+\xi_0}{(1+\xi^2)^{\frac{1}{2}}}. \tag{1}$$

Here $\overline{u_e^0}(s,t)$ denotes a dimensionless velocity $u_e^0/u_\infty(1+t_1)$, the parameter ξ denotes a dimensionless distance from the nose related to the x- and y-coordinates of the ellipse

by $x+a = \frac{1}{2}at_1^2\xi^2$, $y = at_1^2\xi$, and $\xi_0(\equiv \alpha/t_1)$ represents a dimensionless angle of attack. The parameter ξ is related to the surface distance s by

$$s = at_1^2 \int_0^{\xi} (1+\xi^2)^{\frac{1}{2}} \mathrm{d}\xi.$$

The boundary-layer equations for unsteady incompressible laminar flows on oscillating airfoils are well known and can be written as

$$\frac{\partial u}{\partial s}+\frac{\partial v}{\partial n} = 0, \tag{2}$$

$$\frac{\partial u}{\partial t}+u\frac{\partial u}{\partial s}+v\frac{\partial u}{\partial n} = \frac{\partial u_e}{\partial t}+u_e\frac{\partial u_e}{\partial s}+\nu\frac{\partial^2 u}{\partial n^2}. \tag{3}$$

Solutions to these equations are usually obtained for prescribed boundary conditions given by

$$n = 0, \quad u = v = 0; \qquad n = n_e, \quad u = u_e(s,t) \tag{4}$$

and we shall refer to this as the standard problem. In the interactive problem we determine $u_e(s,t)$ partly from inviscid theory and partly from the pressure distribution resulting from the blowing velocity $\mathrm{d}/\mathrm{d}s\,(u_e\delta^*)$ induced by the boundary layer. Thus we write

$$u_e(s,t) = u_e^0(s,t)+u_c(s,t), \tag{5}$$

where $u_e^0(s,t)$ is the inviscid velocity and $u_c(s,t)$ is related to the blowing velocity by a variation of the Hilbert integral

$$u_c(s,t) = \frac{1}{\pi}\int_{-\infty}^{\infty} \frac{\mathrm{d}}{\mathrm{d}s}(u_e\delta^*)\frac{\mathrm{d}\sigma}{s-\sigma}, \tag{6}$$

which is valid for straight walls but can be generalized to airfoils as discussed by Cebeci & Clark (1984). The free-stream velocity, consistent with (1), has the form

$$\overline{u_e^0}(s,t) = \frac{\xi+\xi_0(1+A\,\sin\omega^* t)}{(1+\xi^2)^{\frac{1}{2}}}, \tag{7}$$

where A is an amplitude parameter and ω^* is a dimensional frequency.

For attached flows, the effect of $u_c(s,t)$ is generally weak but is enhanced in the neighbourhood of separation, as can be surmised by noting that the integrand in (6) would otherwise develop a strong singularity at separation and cause the solutions to break down further downstream. As discussed by Cebeci *et al.* (1981), it is sufficient to replace (6) by

$$u_c(s,t) = \frac{1}{\pi}\int_{s_a}^{s_b} \frac{(u_e\delta^*)'}{s-\sigma}\mathrm{d}\sigma, \tag{8}$$

where the prime denotes differentiation with respect to s and s_a and s_b denote the beginning and the end of the interaction region.

To complete the formulation of the problem, upstream boundary conditions must be specified in the (t,n)-plane at some $s = s_0$ as well as initial conditions in the plane (s,n) at $t = 0$. If steady-flow conditions prevail at $t = 0$, the initial conditions can be

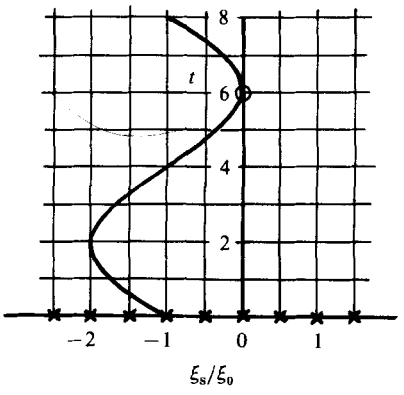

FIGURE 1. Variation of stagnation point with time for one cycle according to (10) with $A = 1$, $\omega^* = \frac{1}{4}\pi$.

obtained easily for both surfaces by solving the conservation equations for steady flow which, in this case, are given by (2) and by

$$u\frac{\partial u}{\partial s}+v\frac{\partial u}{\partial n}=u_e\frac{\mathrm{d}u_e}{\mathrm{d}s}+\nu\frac{\partial^2 u}{\partial n^2}. \tag{9}$$

There is no problem with the initial conditions for (2) and (9) since the calculations start at the stagnation point where they admit similarity solutions.

The generation of the upstream boundary conditions for (5) and (6) requires a special numerical procedure. Since the complete velocity-profile distribution on a previous time line is known, solutions can be determined on the next time line by an explicit method. If we wish to avoid stability problems, however, an implicit method is required and generation of a starting profile on the new time line becomes a problem.

In order to explain the problem further, it is instructive to see what happens to the stagnation point as a function of time. For this purpose let us consider (7). Since $\overline{u_e^0} = 0$ at the stagnation point, its location, ξ_s, based on the external streamlines is given by

$$\xi_s = -\xi_0(1+A\sin\omega^* t). \tag{10}$$

Figure 1 shows the variation of the stagnation point with time for one cycle according to (10), with $A = 1$, $\omega^* = \frac{1}{4}$. We see that when $t = 2$, the stagnation point ξ_s is at $-2\xi_0$, and when $t = 6$, it is at 0, etc. If ξ_s were fixed, we could assume that $u = 0$ at $\xi = -\xi_0$ for all time and all n, but this is not the case. It is also possible to assume that the stagnation point is coincident with zero u-velocity for a prescribed time but we should note that the stagnation point defined by (10) is based on the vanishing of the external velocity. For a time-dependent flow, this does not imply that the u-velocity must be zero across the layer at a given ξ-location and specified time; indeed flow reversals can occur owing to the movement of the locus of zero u-velocity across the layer and can cause numerical instabilities which require the use of special numerical schemes as discussed by Cebeci & Carr (1981).

3. Solution procedure

With the upstream boundary conditions determined by the procedure of Cebeci & Carr (1981) and with the initial conditions obtained from the solution of (2) and (9)

subject to the boundary conditions given by (4)–(6), (2) and (3) can be solved for both standard or inverse problems. In practice a standard procedure is used up to a specified ξ-location after which the calculations may proceed by either standard or inverse procedures. For example, the evolution of the boundary layer on an oscillating airfoil with prescribed pressure distribution is determined with the standard procedure and the inverse procedure is used after a short distance from the leading-edge region where the inviscid- and viscous-flow equations are solved interactively.

To solve the equations for both standard and inverse problems we use modified forms of Keller's box scheme. The Mechul function formulation of Cebeci (1976) is used in the inverse case and treats the external velocity as an unknown. Before we describe this formulation and the solution procedure, it is convenient to write (2)–(4) in a form more suitable for computation. To achieve this we define dimensionless distances η and $\bar{s}$ and time τ by

$$\eta = \left[\frac{R(1+t_1)}{2t_1^2}\right]^{\frac{1}{2}} \frac{n}{a}, \quad \bar{s} = \frac{s}{at_1^2}, \quad \tau = \frac{u_\infty(1+t_1)}{at_1^2}t, \tag{11a}$$

with $R = 2au_\infty/\nu$, and a dimensionless stream function f by

$$\psi(s, n, t) = [(1+t_1)au_\infty \nu t_1^2]^{\frac{1}{2}} f(\bar{s}, \eta, \tau). \tag{11b}$$

These relations may be introduced into (2) and (3) to give, with primes denote differentiation with respect to η,

$$f''' + \frac{\partial w}{\partial \tau} + w\frac{\partial w}{\partial \bar{s}} = \frac{\partial f'}{\partial \tau} + f'\frac{\partial f'}{\partial \bar{s}} - f''\frac{\partial f}{\partial \bar{s}}, \tag{12}$$

where

$$w = \frac{u_e}{u_\infty(1+t_1)}, \quad f' = \frac{u}{u_\infty(1+t_1)}.$$

The boundary conditions follow from (4)–(6) and can be written as

$$\left.\begin{aligned} &\eta = 0, \quad f = f' = 0; \\ &\eta = \eta_e, \quad f' = w, \quad w = \overline{u_e^0} + \epsilon \int_{\bar{s}_a}^{\bar{s}_b} \frac{\mathrm{d}\Delta}{\mathrm{d}\bar{s}} \frac{\mathrm{d}\bar{\sigma}}{\bar{s}-\bar{\sigma}}. \end{aligned}\right\} \tag{13}$$

Here Δ denotes a dimensionless displacement thickness given by

$$\Delta(\bar{s}, \tau) = \eta_e w - f_e \tag{14}$$

and ϵ is a parameter defined by

$$\epsilon = \frac{1}{\pi t_1}\left[\frac{2}{R(1+t_1)}\right]^{\frac{1}{2}}. \tag{15}$$

To pave the way for the description of the numerical method, we define a new variable

$$\theta = \frac{\partial f}{\partial \bar{s}} \tag{16}$$

and write (12) as

$$f''' + f''\theta + \frac{\partial w}{\partial \tau} + w\frac{\partial w}{\partial s} = \frac{\partial f'}{\partial \tau} + f'\frac{\partial f'}{\partial s}, \tag{17}$$

where the overbar has been omitted. We use Keller's (1974) box method to solve this

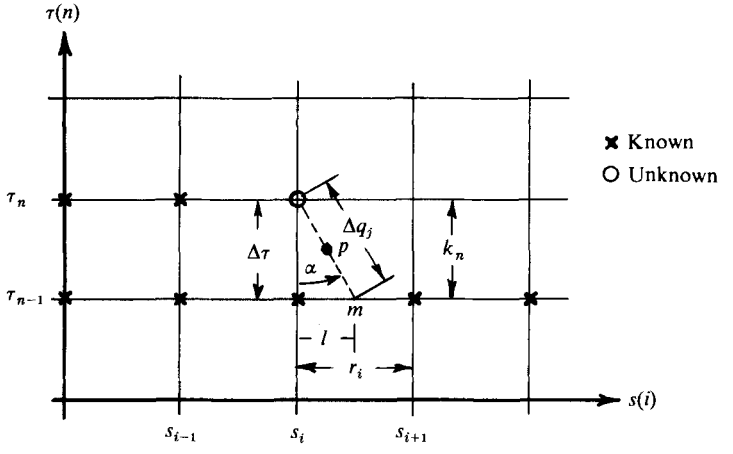

FIGURE 2. Notation for the characteristic box scheme.

equation. In regions of no flow reversal the so-called standard box method is used, and where there is flow reversal this is replaced by the characteristic scheme that is based on the solution of (17) along streamlines as described by Keller (1978) and Cebeci (1986). This scheme allows the step sizes in the τ- and s-directions to be automatically adjusted to ensure that the region of backflow determined by the local streamlines does not violate a condition like the Courant, Friedrichs and Lewy (CFL) stability criterion defined by $\beta = l/\Delta\tau$ (see figure 2). Although the zigzag scheme of Krause, Hirschel & Bothemann (1968) can also be used for this purpose, it can be inaccurate in regions of large flow reversal since the orientation of the numerical mesh is chosen *a priori*, as discussed by Cebeci (1986) and later in this paper.

To solve (17) and (14) with the box scheme and the Mechul function formulation, we let

$$f' = e \tag{18}$$

and introduce a new function g defined by

$$e' = g \tag{19a}$$

and, with $w(x)$ treated as unknown

$$w' = 0, \tag{19b}$$

write (16) and (17) and their boundary conditions as

$$\theta' = \frac{\partial e}{\partial s}, \tag{19c}$$

$$g' + g\theta + \frac{\partial w}{\partial \tau} + w\frac{\partial w}{\partial s} = \frac{\partial e}{\partial \tau} + e\frac{\partial e}{\partial s}, \tag{19d}$$

$$\left.\begin{aligned} &\eta = 0, \quad f = e = 0; \\ &\eta = \eta_e, \quad e = w, \quad w = \overline{u_e^0} + \epsilon \int_{s_a}^{s_b} \frac{\mathrm{d}\Delta}{\mathrm{d}s} \frac{\mathrm{d}\sigma}{s-\sigma}. \end{aligned}\right\} \tag{20}$$

To write the difference equations for the system given by (19) and (20), we consider a net cube in which the net points are denoted by

$$\left.\begin{aligned} s_0 &= 0, \quad s_i = s_{i-1} + r_i \quad (i = 1, 2, \ldots, I), \\ \tau_0 &= 0, \quad \tau_n = \tau_{n-1} + k_n \quad (n = 1, 2, \ldots, N), \\ \eta_0 &= 0, \quad \eta_j = \eta_{j-1} + h_j \quad (j = 1, 2, \ldots, J), \end{aligned}\right\} \tag{21}$$

where $r_i = \Delta s_i$, $k_n = \Delta \tau_n$ and $h_j = \Delta \eta_j$.

The difference approximations to represent (19a, b) are obtained by averaging about the midpoint $(s_i, \tau_n, \eta_{j-\frac{1}{2}})$,

$$h_j^{-1}(e_j^{i,n} - e_{j-1}^{i,n}) = g_{j-\frac{1}{2}}^{i,\eta}, \tag{22a}$$

$$h_j^{-1}(w_j^{i,n} - w_{j-1}^{i,n}) = 0, \tag{22b}$$

where, for example,

$$e_{j-\frac{1}{2}}^{i,\eta} = \tfrac{1}{2}(e_j^{i,n} + e_{j-1}^{i,n}). \tag{23}$$

The finite-difference approximations to (19c, d) are obtained by centring all quantities except θ at the centre of the cube $(s_{i-\frac{1}{2}}, \tau_{n-\frac{1}{2}}, n_{j-\frac{1}{2}})$ by taking the values of each, say q, at the four corners of the box; that is,

$$q_{j-\frac{1}{2}}^{i-\frac{1}{2},n} = \tfrac{1}{2}(q_{j-\frac{1}{2}}^{i,\eta} + q_{j-\frac{1}{2}}^{i-1,n}) = \tfrac{1}{4}(q_j^{i,n} + q_{j-1}^{i,n} + q_{j-1}^{i-1,n}). \tag{24a}$$

The centring of θ is done by writing it as

$$\theta_{j-\frac{1}{2}}^{i-\frac{1}{2},n-\frac{1}{2}} = \tfrac{1}{2}(\theta_j^{i-\frac{1}{2},n} + \theta_{j-1}^{i-\frac{1}{2},n-\frac{1}{2}}). \tag{24b}$$

In this notation, the difference approximations to (19c, d) can be written in the form

$$h_j^{-1}(\theta_j - \theta_{j-1}) = r_i^{-1}(\bar{e}_i - \bar{e}_{i-1}), \tag{25a}$$

$$\begin{aligned} h_j^{-1}(\bar{g}_j - \bar{g}_{j-1}) + \bar{g}_{j-\frac{1}{2}}\theta_{j-\frac{1}{2}} + k_n^{-1}(\bar{w}_n - \bar{w}_{n-1}) + r_i^{-1}[\bar{w}_{j-\frac{1}{2}}(\bar{w}_i - \bar{w}_{i-1})] \\ = k_n^{-1}(\bar{e}_n - \bar{e}_{n-1}) + r_i^{-1}[\bar{e}_{j-\frac{1}{2}}(\bar{e}_i - \bar{e}_{i-1}) - \bar{g}_{j-\frac{1}{2}}(\bar{f}_i - \bar{f}_{i-1})], \end{aligned} \tag{25b}$$

where, for example,

$$\bar{e}_j = e_j^{i-\frac{1}{2},n-\frac{1}{2}}, \quad \bar{e}_n = e_{j-\frac{1}{2}}^{i-\frac{1}{2},n}, \quad \bar{e}_i = e_{j-\frac{1}{2}}^{i,\eta-\frac{1}{2}}, \quad \theta_j = \theta_j^{i-\frac{1}{2},n-\frac{1}{2}}. \tag{26}$$

Following the procedure of Cebeci *et al.* (1981) the boundary condition involving the Hilbert integral in (20) can be written in the form

$$w_J^{i,n} - c_{ii}\epsilon(\eta_J w_J^{i,n} - f_J^{i,n}) = T_J^{i,n}, \tag{27}$$

where c_{ii} is the matrix of interaction coefficients defining the relationship between the dimensionless displacement thickness and external flow, and the parameter $T_J^{i,n}$ represents terms where values are assumed to be known. It is given by

$$T_J^{i,n} = (\overline{u_e^0})^{i,n} + \epsilon \sum_{m=1}^{i-1} C_{im}\Delta_J^{m,n} + \epsilon \sum_{m=i+1}^{I} C_{im}\Delta_J^{m,n}. \tag{28}$$

To compute the additional unknown of (27), we write (18) in the form

$$h_j^{-1}(f_j^{i,n} - f_{j-1}^{i,n}) = e_{j-\frac{1}{2}}^{i,\eta} \tag{29}$$

so that the system consisting of (22), (25) and (29) can be solved subject to the boundary conditions given by (27) and which follow from (20),

$$f_0 = \theta_0 = e_0 = 0; \quad e_J = w_J. \tag{30}$$

The above system can be linearized by Newton's method and the resulting linear system solved by the block elimination procedure described in Cebeci & Bradshaw (1984) for both standard and inverse formulations. In the former case, it is sufficient to set $\epsilon = 0$ in (27) so that w is equal to $\overline{u_e^0}$.

We follow the above solution procedure when there is no flow reversal across the layer. If separation is identified from the values of $u_j^{i,n}$, we use the characteristic scheme that has recently been described by Cebeci (1986) in relation to the standard problem of computing the impulsively started laminar flow over a circular cylinder. The solution procedure in this case is similar, with small adjustments resulting from the manner in which the difference equations are adjusted to the modified form of (19*d*). Noting the definition of local streamlines, we write

$$\mathrm{d}\tau = \frac{\mathrm{d}s}{e} \tag{31}$$

If we denote distance in this direction by q and the angle that it makes with the τ-axis by α, then (19*d*) can be written as

$$g' + g\theta + \gamma = \lambda \frac{\partial e}{\partial q}, \tag{32}$$

where

$$\lambda = (1+e^2)^{\frac{1}{2}}, \quad \alpha = \tan^{-1} e, \quad \gamma = \frac{\partial w}{\partial \tau} + w\frac{\partial w}{\partial s}. \tag{33a,b,c}$$

The finite-difference approximations to (32) are written along the streamline direction (see figure 2) at

$$\tfrac{1}{2}h_j^{-1}(g_j^{i,n} - g_{j-1}^{i,n}) + \tfrac{1}{2}h_j^{-1}(g_j^{m,n-1} - g_{j-1}^{m,n-1}) + \gamma^p + \tfrac{1}{2}(g_{j-\frac{1}{2}}^{i,\eta} + g_{j-\frac{1}{2}}^{m,n-1})\,\theta_{j-\frac{1}{2}}^p = \tfrac{1}{2}(\lambda_{j-\frac{1}{2}}^{i,\eta} + \lambda_{j-\frac{1}{2}}^{m,n-1})\frac{e_{j-\frac{1}{2}}^{i,\eta} - e_{j-\frac{1}{2}}^{m,n-1}}{\Delta q_{j-\frac{1}{2}}}, \tag{34}$$

where

$$\Delta q_{j-\frac{1}{2}} = \frac{k_n}{\cos\alpha_{j-\frac{1}{2}}}. \tag{35}$$

The relation between $\theta_{j-\frac{1}{2}}^p$ and those values of θ centred at $(i-\frac{1}{2}, n-\frac{1}{2})$ and $(i-\frac{3}{2}, n-\frac{1}{2})$ are

$$\theta_{j-\frac{1}{2}}^p = \frac{\theta_{j-\frac{1}{2}}^{i-\frac{3}{2}} - \theta_{j-\frac{1}{2}}^{i-\frac{1}{2}}}{s_{i-\frac{3}{2}} - s_{i-\frac{1}{2}}}(s^p - s_{i-\frac{3}{2}}) + \theta_{j-\frac{1}{2}}^{i-\frac{3}{2}}. \tag{36}$$

The solution of (12) subject to the boundary conditions given by (13) is achieved by solving the system of equations given by (18), (19) and (20) (standard scheme) when there is no flow reversal. When calculated results reveal flow reversal ($e_j < 0$), further iterations at that location make use of the characteristic scheme that seeks the solution of (18), (19*a*, *b*, *c*) and (32) for $e_j < 0$ and the regular scheme for $e_j < 0$. This switch from one scheme to another continues to allow quadratic convergence and ensures that numerical instabilities are avoided provided that the step lengths in the τ- and s-directions are 'properly' selected, as we shall discuss in the following section.

4. The question of singularity on an oscillating airfoil

The problem of a circular cylinder impulsively started from rest has served as a model problem with which to examine unsteady boundary layers and the nature of the solutions in the presence of large flow reversal. Noteworthy contributions have been made by Cebeci (1979), van Dommelen & Shen (1982), Cowley (1983) and Ingham (1984), and show that at large times the distribution of displacement thickness has a steep rise near the location of zero wall shear, with a consequent tendency for calculations to break down. The suggested values for the time and location of zero wall shear and peaking of the displacement velocity, $[\mathrm{d}/\mathrm{d}s(u_e\delta^*)]$ vary. The explanation for the breakdown of the calculations has been provided by Cebeci (1986) who demonstrated that numerical calculations must satisfy a CFL-like stability criterion. If this is done, it is expected that the location of the singularity associated with unsteady flow and large time will correspond exactly to that of steady flow, namely $\theta = 105°$, rather than $\theta = 111°$. The same situation cannot be expected with oscillating airfoils where the solutions are cyclic and do not tend to a steady state.

The present study examines the nature of solutions to the boundary-layer equations for the flow on an oscillating airfoil, which can give rise to extensive regions of flow reversal and separation. Here flow reversal implies the existence of negative wall shear, and separation is taken to correspond to situations where calculations with a prescribed pressure distribution break down owing to a singularity. The calculations were made for three values of reduced frequency ω, with $\xi_0 = 1$ and $A = \frac{1}{2}$. With the choice of $\omega = 0.001$, 0.01 and 0.10, the maximum value of ξ_{eff}, defined by

$$\xi_{\text{eff}} = \xi_0(1 + A \sin \omega^* t),$$

is sufficient to provoke separation with a strong singularity. For example, the maximum value of ξ_{eff} is 1.5 at $\omega\tau = 270°$ and the flow conditions closely resemble a steady separated flow at the smaller frequencies $\omega = 0.001$ and 0.01. Since the value of ξ_{eff} corresponding to steady flow separation is 1.115, we would expect the calculations to break down before $\omega\tau = 270°$ owing to the singularity. For the higher frequency case ($\omega = 0.10$), we expect the solutions to break down later than $\omega\tau = 270°$ with flow reversals occurring in the range $270° < \omega\tau < 360°$.

The calculations were arranged to parallel those previously performed for a circular cylinder and reported by Cebeci (1986). Thus both the zigzag and the characteristic-box schemes were used first with time and distance steps that were chosen arbitrarily and subsequently with values in agreement with the stability criterion. The results of figure 3 for $\omega = 0.10$ were obtained with the zigzag box scheme by Cebeci, Khattab & Schimke (1984) for a $\Delta\xi$ spacing specified such that $\Delta\xi_i = 0.01$ up to $\xi = 1.7$, $\Delta\xi_i = 0.005$ for $1.7 < \xi < 4$ and $\Delta\xi_i = 0.01$ for $4 < \xi < 8$; the time steps k_n were 10 degrees for $0 < \omega\tau < 260°$, 5 degrees for $260° < \omega\tau < 295°$, and 1.25 degrees for $295° < \omega\tau < 360°$. The calculations broke down at $\omega\tau = 310°$, indicating flow separation at this location.

Figure 3(*a*) shows that the variation of the displacement thickness

$$\tilde{\delta}^* = \frac{\delta^*}{a}\frac{1}{\epsilon\pi\tau_1^2}$$

is generally smooth except in the neighbourhood of $\xi = 2.12$ and for $\omega\tau = 308.75°$. The first sign of irregularity is the steepening of the slope of $\tilde{\delta}^*$ when $\omega\tau = 300°$, and

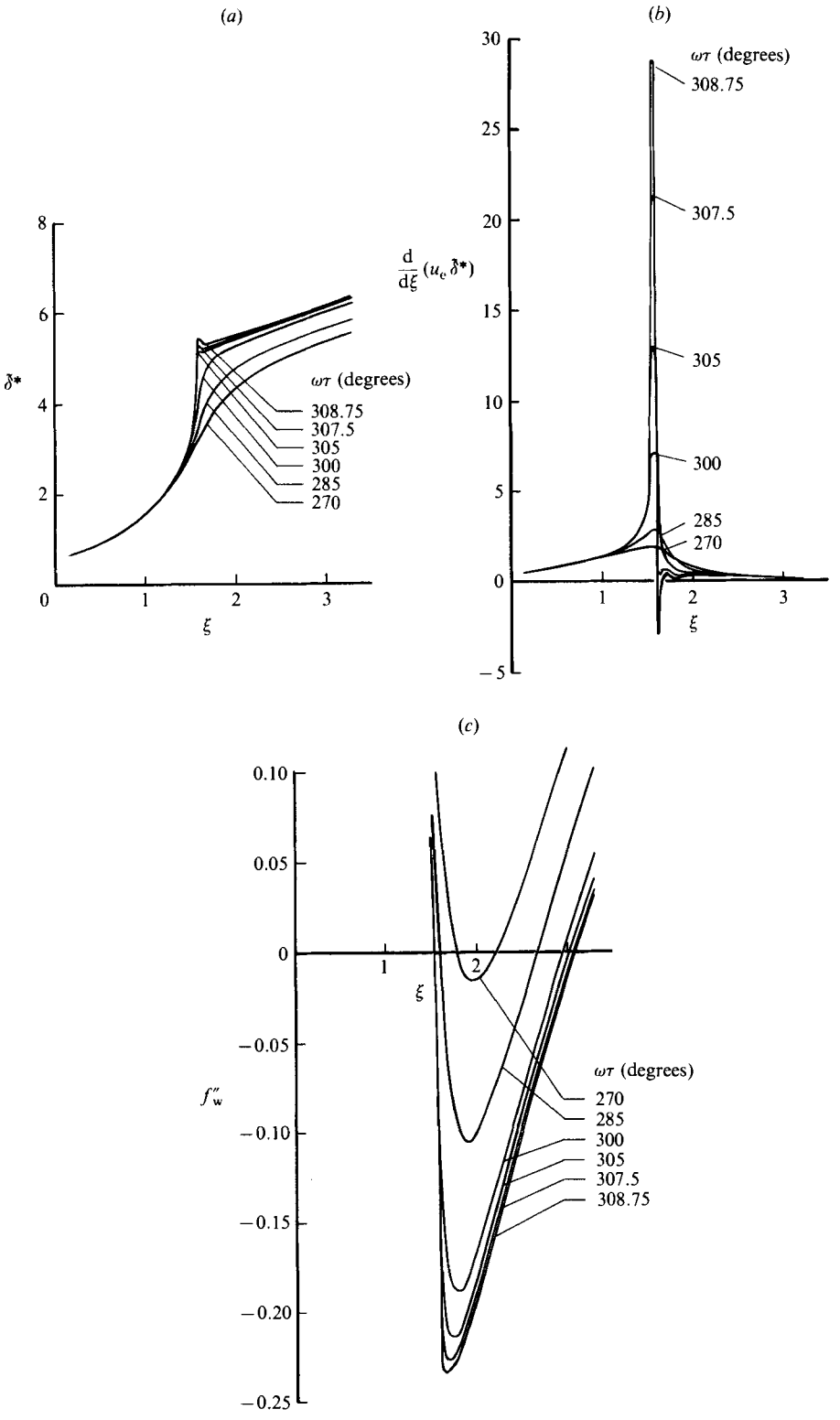

FIGURE 3. Variation of (*a*) displacement thickness $\tilde{\delta}^*$, (*b*) displacement velocity $d/d\xi(u_e\tilde{\delta}^*)$, and (*c*) wall-shear parameter f''_w with ξ for the oscillating airfoil; $A = 1$, $\omega = 0.1$.

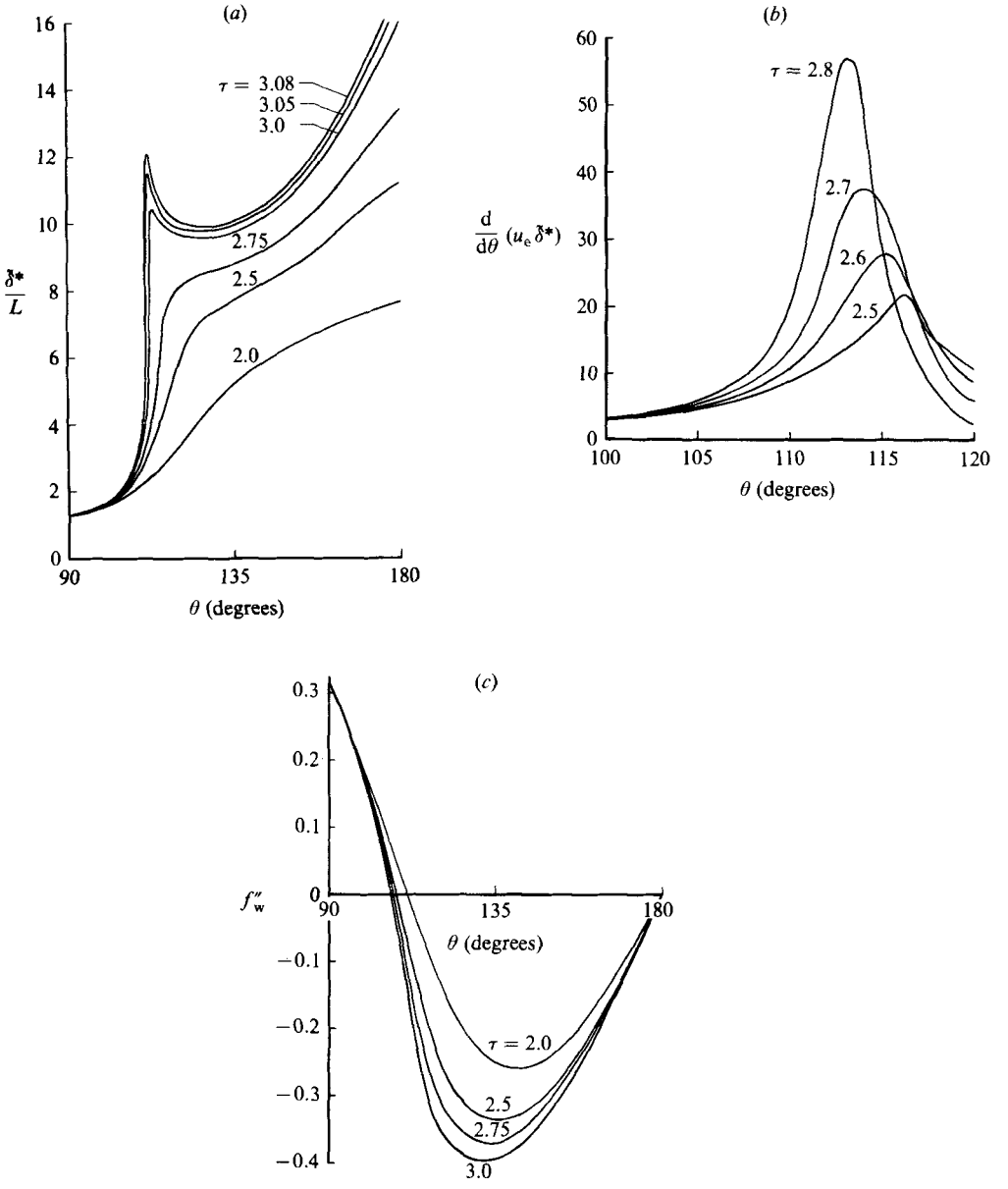

FIGURE 4. Variation of (*a*) displacement thickness $\tilde{\delta}^*$, (*b*) displacement velocity, and (*c*) wall-shear parameter with θ for the circular cylinder.

a local maximum of $\tilde{\delta}^*$ occurs at $\xi = 2.12$ when $\omega\tau = 308.75°$. When the same results are plotted for a displacement velocity, $(\mathrm{d}/\mathrm{d}\xi)\,(u_e\tilde{\delta}^*)$ (figure 3*b*) we observe that the steepening of the displacement velocity as the peak moves from $\xi = 2.125$ to 2.08 with $\omega\tau$ changing from 300° to 308.75°. It should be noted that the maximum value of displacement velocity moves towards the separation point with increasing $\omega\tau$ and the same behaviour will be shown to occur for the circular cylinder discussed below. As shown in figure 3(*c*), the wall-shear parameter f''_w shows no signs of irregularity for

$\omega\tau$	k_n
0–240°	10°
240–255°	5°
255–261°	3°
261–265°	2°
265–284°	1°
284–305°	0.5°
305–320°	0.25°
320–360°	0.5°

TABLE 1. The distribution of step sizes in $\omega\tau$ for $\omega = 0.1$ in accordance with the requirements of the stability parameter β

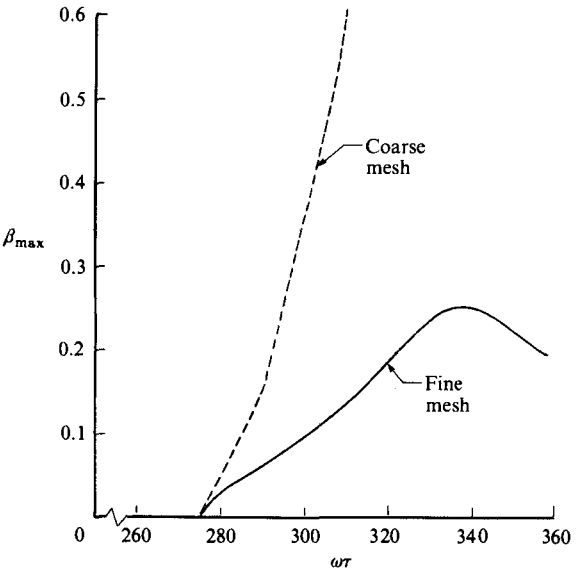

FIGURE 5. Effect of the coarse and fine meshes on the variation of the stability parameter β with $\omega\tau$.

$\omega\tau \leqslant 308.75°$ but a deep minimum in f''_w occurs near $\xi = 2.15$, i.e. near the peak of $\tilde{\delta}^*$.

It is interesting and useful to compare the results presented in figure 3 for an oscillating airfoil with those obtained by Cebeci (1982) for a circular cylinder started impulsively from rest, figure 4, and obtain with the same zigzag scheme. As in the case of the oscillating airfoil, the flow reverses and remains smooth up to the separation point. However, just downstream of separation with increasing time, a singularity seems to develop in the neighbourhood of $\theta = 112°$ and $\tau \approx 3.0$ and it was not possible to continue the boundary-layer calculations beyond this time and angular location. From figure 4(*a*) we see that the variation of displacement thickness is smooth for values of θ less than 108° and it begins to steepen thereafter. The same results are plotted in figure 4(*b*) to demonstrate that the displacement velocity exhibits a maximum which increases rapidly with time, as in figure 3(*b*), with the maximum shifting towards the location of separation with increasing time. The results of local skin-friction coefficients, figure 4(*c*), follow similar trends to those

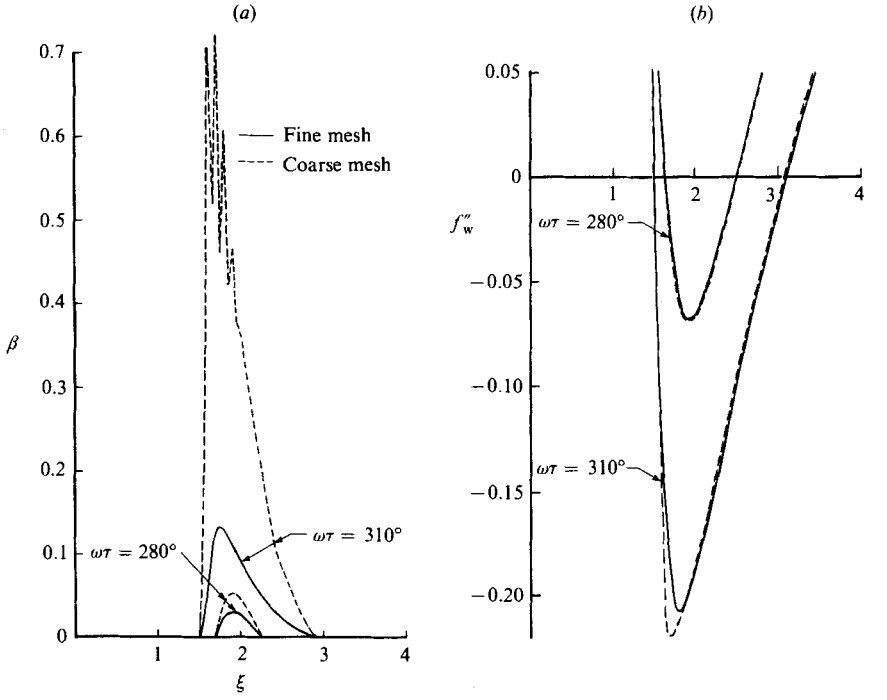

FIGURE 6. Effect of the coarse and fine meshes on the variation of the (*a*) stability parameter β and (*b*) wall shear f''_w with ξ.

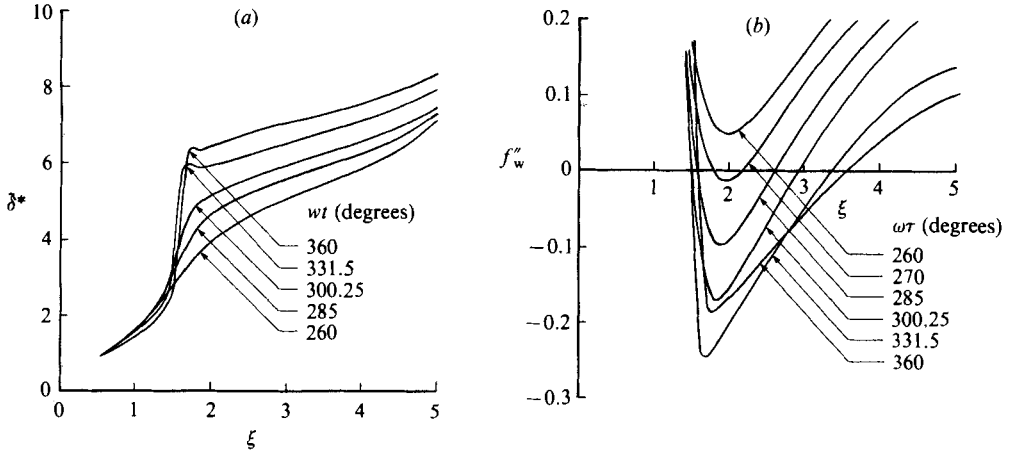

FIGURE 7. Results obtained with the characteristic-box scheme for $\omega = 0.1$. Variation of (*a*) displacement thickness δ^* and (*b*) wall shear f''_w with ξ.

obtained for the oscillating airfoil with the distributions passing through zero with no signs of irregularity and no breakdown before the time corresponding to the singularity.

The calculations that led to figure 3 were repeated with the characteristic-box scheme using the same coarse variations of k_n and $\Delta\xi_i$, and the results were identical with those obtained with the zigzag scheme up to $\omega\tau = 280°$. At $\omega\tau = 282.5°$, the solutions of the zigzag scheme were smooth and free of wiggles but those of the

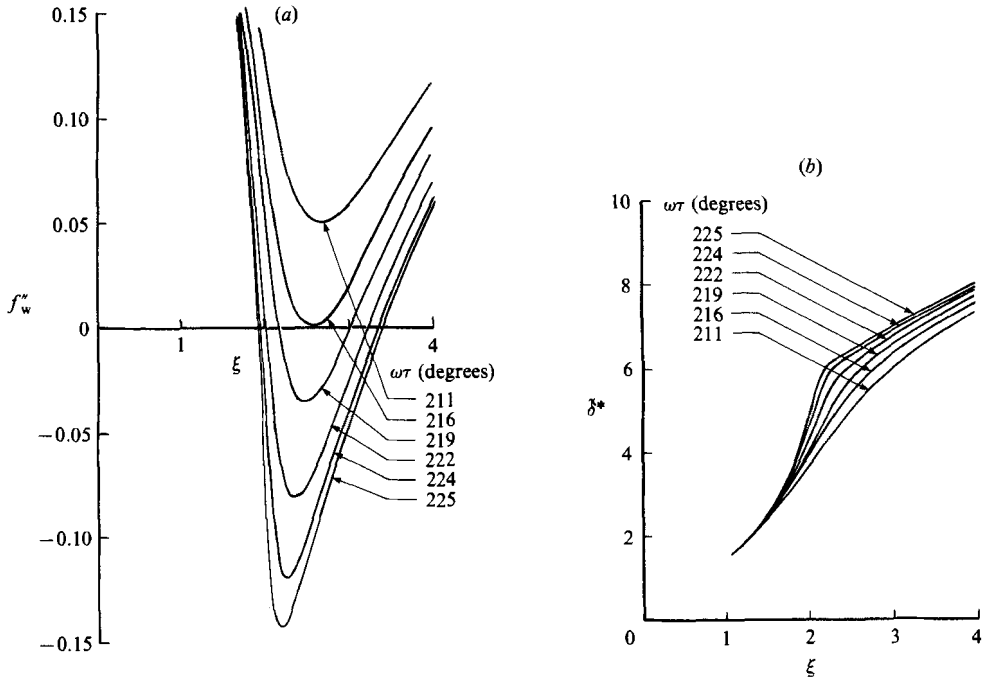

FIGURE 8. Variation of (*a*) wall shear f''_w and (*b*) displacement thickness δ^* with ξ for $\omega = 0.01$.

characteristic-box scheme exhibited oscillations in f''_w which led to their breakdown. The solutions with the zigzag scheme, however, continued without numerical difficulties until $\omega\tau = 310°$, where oscillations appeared and led to the breakdown of the solutions at the next time step.

The characteristic box was used subsequently with values of $\Delta\xi_i$ fixed as before and with values of k_n determined in accord with the stability requirement as shown in table 1. This procedure avoided the breakdown of the solutions and, as can be seen from figure 5, the maximum value of β increases considerably with $\omega\tau$ so that the solutions required correspondingly smaller values of the time step. It is interesting to note that the wall-shear distributions of figure 6 are uninfluenced by the mesh at $\omega\tau = 280°$ and 310° but, for $\omega\tau > 310°$, the coarse mesh leads to large values of β and breakdown of the solutions.

Figure 7 (*a*) shows the distributions of displacement thickness for values of $\omega\tau$ from 260° up to 360° and completes the cycle. The results up to 300° were identical with those of figure 3 (*a*) with rapid increase of the displacement thickness corresponding to the increasing extent of flow reversal, as shown by the wall-shear distributions of figure 7 (*b*). It can also be seen from this figure that the maximum displacement thickness and minimum wall shear move upstream with increasing $\omega\tau$ for values of $\omega\tau$ up to 324.5°; this feature was also observed in the calculations performed for the circular cylinder and shown in figure 4. The results obtained with the zigzag scheme and values of k_n determined by the characteristic scheme for the oscillating airfoil were identical with those discussed above, and similar correspondence was obtained with the calculations performed for the circular cylinder.

Figures 8 and 9 show the distributions of wall shear and displacement thickness for two smaller frequencies, $\omega = 0.01$ and 0.001. As expected, the critical value of the

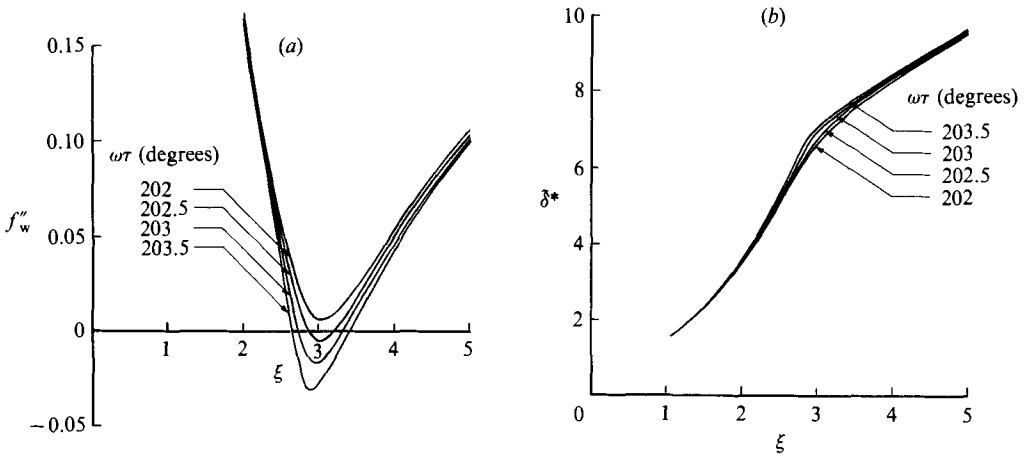

FIGURE 9. Variation of (*a*) wall shear f''_w and (*b*) displacement thickness $\tilde{\delta}^*$ with ξ for $\omega = 0.001$.

reduced angle that corresponds to separation is smaller than that for the higher frequency and closer to that of the steady state, $\xi = 1.16$. For $\omega = 0.01$, the breakdown of the solutions occurs at $\omega\tau = 226°$, which corresponds to an effective reduced angle of $\xi_{\text{eff}} = 1.360$; for $\omega = 0.001$, the corresponding values are $\omega\tau = 204°$ and 1.203. We also note from figure 8(*a*, *b*) that the flow is a 'little' unsteady even at these frequencies, and the solutions do not break down with the appearance of flow reversal, which increases in extent as ω changes from 0.001 and 0.01.

5. Interaction as an answer to the question of singularity

The interaction procedure discussed in § 3 has been applied to the flow problem examined in § 4 with the standard method, and the results are shown in figures 10–14 and discussed below. In contrast to the standard problem, which makes the implicit assumption of infinite Reynolds number, the interaction requires specification of a finite Reynolds number. A thickness ratio t_1 has also to be specified and, since the definition of ϵ involves R and t_1, the calculations are performed for specified values of ϵ. In all cases shown, the calculations made use of time steps determined by the characteristic scheme in agreement with the stability requirement. This was not done in the calculations of Cebeci *et al.* (1984) and the solutions exhibited oscillations which stemmed from the numerical method.

The present calculations were performed in the following way. For all values of time, with $\omega\tau$ ranging from 0° to 360°, the standard method and the leading-edge-region procedure of Cebeci & Carr (1981) were used to generate initial conditions at a short distance from the leading edge, $\xi = 0.5$. With these initial conditions and for each value of $\omega\tau$, the inverse method was used to calculate the unsteady flow from $\xi = 0.5$ to 10, for the specified value of ϵ. Since the system of equations is now elliptic, sweeps in the ξ-direction were necessary to achieve a converged solution; around three sweeps were required where flow reversal was encountered and a single sweep sufficed where it did not. It is to be expected that the value of ϵ will influence the number of sweeps and, since it is linked to physical parameters, will affect the singularity and the size of the bubble.

Figures 10 and 11 show the results for $\omega = 0.001$ and 0.01 with $\epsilon = 3 \times 10^{-3}$. They are nearly the same as those obtained by the standard method and shown in figures

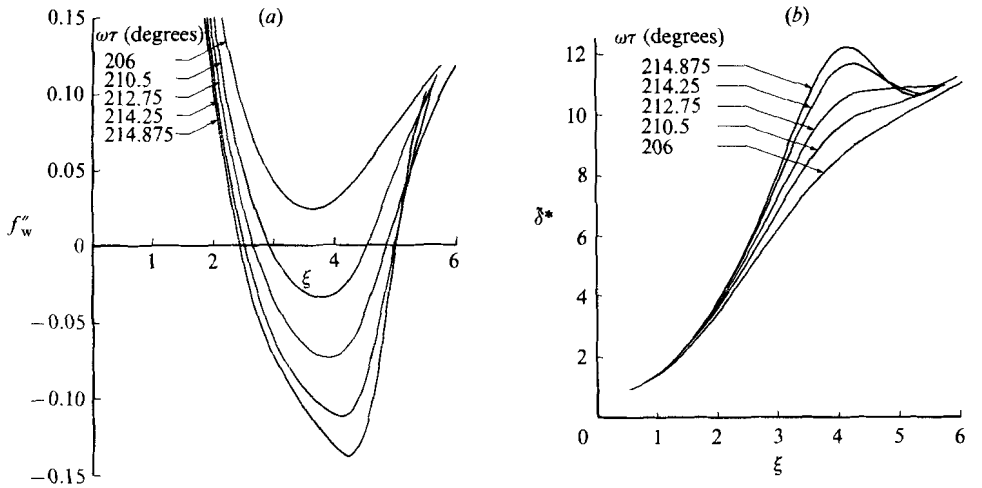

FIGURE 10. Effect of interaction on the variation of (*a*) wall shear f''_w and (*b*) displacement thickness $\tilde{\delta}^*$ for $\omega = 0.001$ and $\epsilon = 3 \times 10^{-3}$.

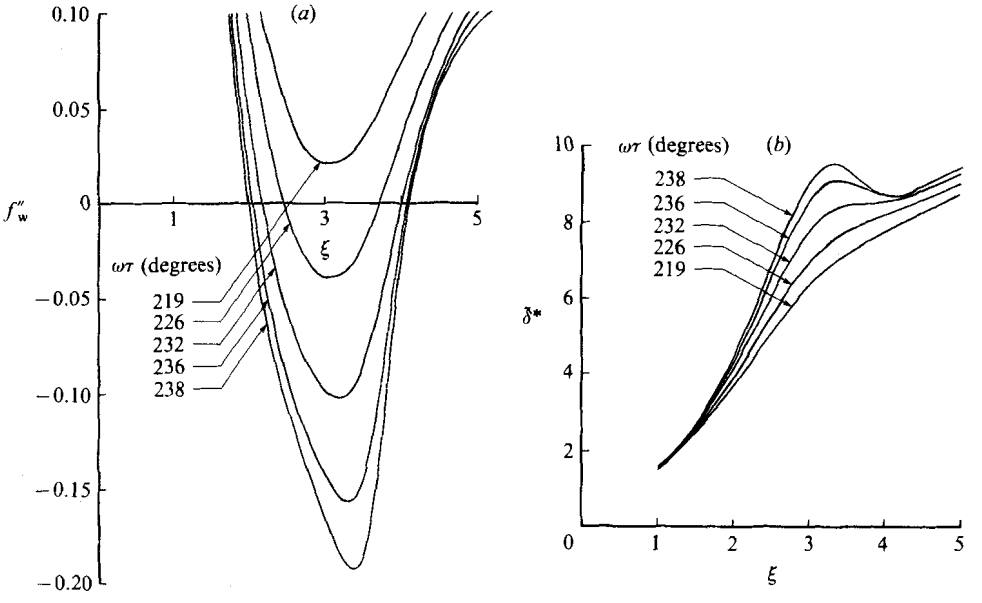

FIGURE 11. Effect of interaction on the variation of (*a*) wall shear f''_w and (*b*) displacement thickness $\tilde{\delta}^*$ with ξ for $\omega = 0.01$ and $\epsilon = 3 \times 10^{-3}$.

8 and 9 prior to flow reversal where the influence of the Reynolds number is small and increase after flow reversal. In the case of $\omega = 0.001$, for example, the standard method predicts flow reversal around $\xi_{\text{eff}} = 1.19$ (see figure 9), and with interaction (figure 10) this effective angle is between 1.219 and 1.254. The maximum negative value of the wall-shear parameter f''_w obtained with the standard method is around -0.03 at $\xi_{\text{eff}} = 1.199$ and may be compared with the maximum value of f''_w of -0.14 at $\xi_{\text{eff}} = 1.286$ obtained with interaction. As expected, the interaction allows the calculations to be performed at higher angles of attack than those achieved with the standard method. For $\omega = 0.001$, the maximum α_{eff} for which calculations can

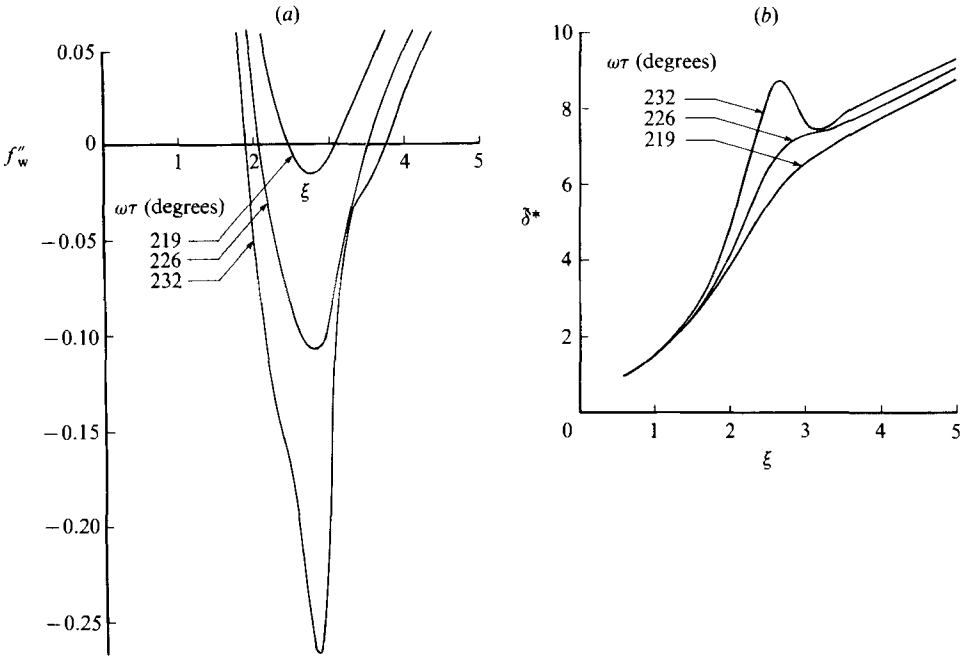

FIGURE 12. Effect of interaction on the variation of (*a*) wall shear f''_w and (*b*) displacement thickness δ^* with ξ for $\omega = 0.01$ and $\epsilon = 10^{-3}$.

be performed with the standard method is 1.199 with breakdown occurring at $\xi_{\text{eff}} = 1.209$; the corresponding values with interaction are 1.286 and 1.287. Comparison of wall-shear results with both procedures and $\omega = 0.001$ indicates that the extent of the recirculation region $\Delta\xi$ is around 0.5 for the standard case, and around 2.5 for the interactive case. The solutions do not have a singularity in the former case but do contain flow reversals, and this suggests that time-dependent flows can be calculated without using an inverse procedure. As the angle of attack exceeds $\xi_{\text{eff}} = 1.199$ for $\omega = 0.001$, a singularity develops and requires an inverse procedure as in two-dimensional steady flows. This procedure allows the calculation of larger regions of reverse flow where the flow is now separated.

We see a similar picture with the greater unsteadiness corresponding to $\omega = 0.01$, for which the standard method allows calculations up to an effective angle of attack of 1.354 (figure 8*a*), a value considerably higher than 1.199 obtained at $\omega = 0.001$. The first flow reversal occurs shortly after $\xi_{\text{eff}} = 1.294$ and breakdown occurs at $\xi_{\text{eff}} = 1.360$ with maximum negative wall shear values of -0.14 at $\xi_{\text{eff}} = 1.354$ and -0.035 at $\xi_{\text{eff}} = 1.315$. The extent of the maximum reverse-flow region is now 1.5, considerably larger than for $\omega = 0.001$, and indicates that the more unsteady nature of the flow produces a bigger region of reverse flow free from singularities. For this value of ω, the interactive scheme increases the value of ξ_{eff} for which solutions can be obtained to 1.424 with breakdown occurring shortly after this value, at 1.428 (see figure 11). The first flow reversal occurs after $\xi_{\text{eff}} = 1.315$ with maximum negative wall shear equal to -0.19 at $\xi_{\text{eff}} = 1.424$, and the extent of the recirculation region has now increased by about 30%. Comparison of maximum wall shear values f''_w at a similar value of ξ_{eff} indicates that those computed with the interactive scheme are lower than those with the standard scheme so that, for example, the interactive

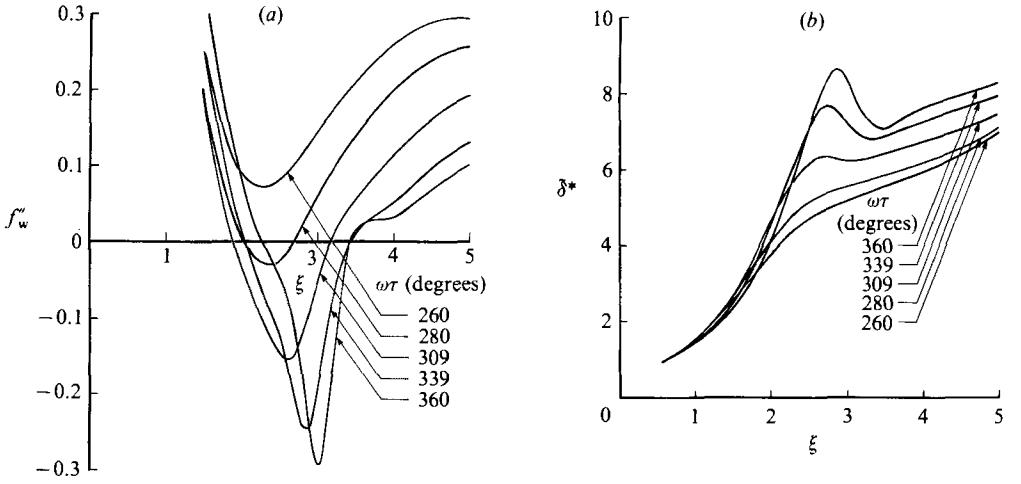

FIGURE 13. Effect of interaction on the variation of (*a*) wall shear f''_w and (*b*) displacement thickness δ^* with ξ for $\omega = 0.1$ and $\epsilon = 3 \times 10^{-3}$.

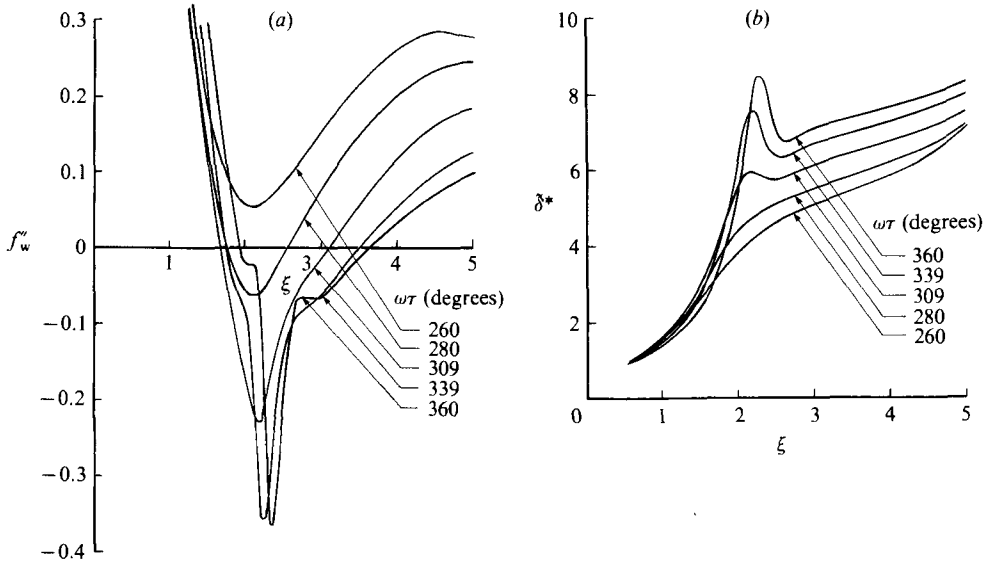

FIGURE 14. Effect of interaction on the variation of (*a*) wall shear f''_w and (*b*) displacement thickness δ^* with ξ for $\omega = 0.1$ and $\epsilon = 10^{-3}$.

scheme gives $(f''_w)_{max} = -0.04$ at $\xi_{eff} = 1.36$ compared with -0.14 at $\xi_{eff} = 1.354$ with the standard method (figure 8*a*).

Figure 12 shows that the size of the reverse-flow region increases with Reynolds number but the effective angle of attack for which solutions can be obtained is only slightly reduced, changing from 1.428 for $\epsilon = 3 \times 10^{-3}$ to around 1.415 for $\epsilon = 10^{-3}$. It is interesting to note that the interactive solutions do not have any flow reversal at $\xi_{eff} = 1.315$ with $\epsilon = 3 \times 10^{-3}$.

Figures 13 and 14 show the results for $\omega = 0.1$ with values of ϵ of 3×10^{-3} and 10^{-3} and they are again similar to those obtained by the standard method, as shown in figure 7, prior to flow reversal where the influence of Reynolds number is small.

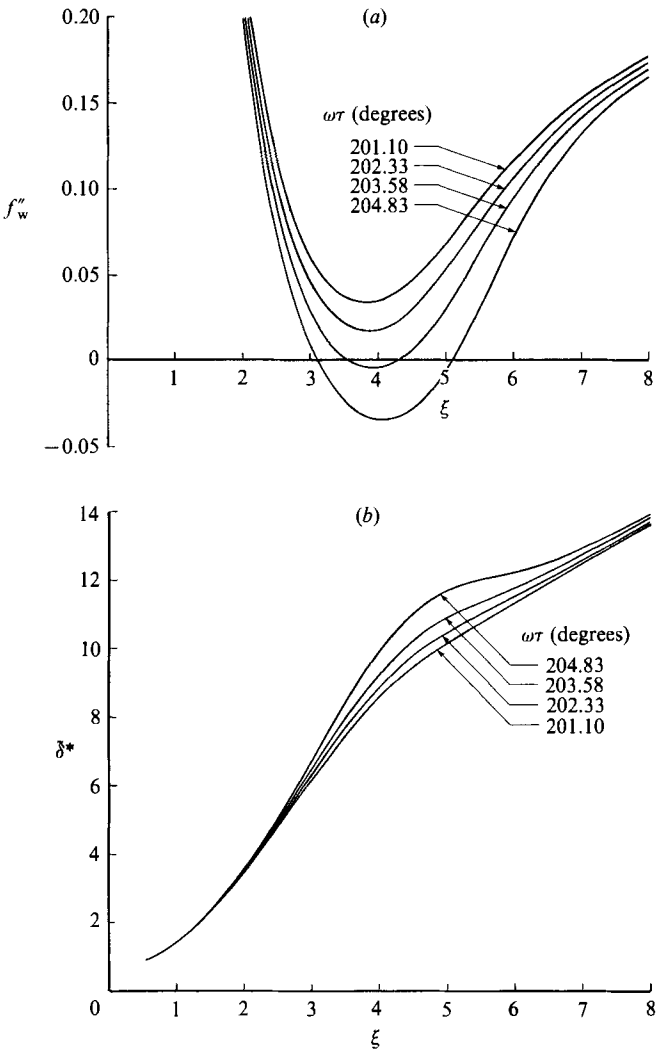

FIGURE 15. Effect of interaction on the variation of (*a*) wall shear f''_w and (*b*) displacement thickness $\tilde{\delta}^*$ for a steady flow at $\epsilon = 3 \times 10^{-3}$.

After flow reversal, the differences between the results obtained with the standard and interactive methods increase as the Reynolds number decreases. It is clear that the solutions are free from the numerical 'wiggles' encountered when the stability criterion was not met.

Comparison of results obtained at the two Reynolds numbers for $\omega = 0.1$ indicates that the interaction does not reduce the maximum negative value of the wall-shear parameter as it did with lower frequencies. For example, f''_w at $\omega\tau = 360°$ is around -0.19 with the standard scheme, and around -0.30 at $\epsilon = 3 \times 10^{-3}$, and around -0.35 at $\epsilon = 10^{-3}$ with the interactive method. The maximum value of negative wall shear calculated with interaction is considerably greater than its corresponding value obtained with the standard method at the end of one complete cycle. Furthermore, the behaviour of the wall shear is not monotonic without interaction so that, for example, f''_w reaches a maximum value equal to -0.25 around $\omega\tau = 331°$ and then

decreases to -0.195 at $\omega\tau = 360°$. With interaction this is not the case, with the maximum negative value of f''_w continuously increasing with $\omega\tau$.

The results of figures 7, 13 and 14 for $\omega = 0.1$ are for an unsteady flow and are unlike those for two other values of ω in that they are free from singularities. For this reason, even though the results in the reverse-flow region and thereafter are different, owing to the Reynolds-number effect, the extent of the reverse-flow region is essentially the same and is consistent with the results obtained at lower frequencies in the absence of flow separation even though the extent of the reverse-flow region is reduced at the lower Reynolds numbers.

Since the calculations began at $\omega\tau = 0°$ with solutions obtained by solving steady-state equations, it was necessary to confirm the extent of their influence. As a consequence, calculations were performed for a second cycle and gave results at $\omega\tau = 720°$ that were identical with those at $\omega\tau = 360°$, confirming that the flow is cyclic. Examination of the results showed that the influence of the initial conditions die out rapidly and have no influence on the solutions presented here.

The results obtained with $\omega = 0.001$ can usefully be compared with the steady-state results of Cebeci *et al.* (1981) shown in figure 15. We might expect that the small unsteadiness associated with this frequency will lead to results very similar to those of steady state. Inspection of figures 10 and 15 shows that, although this is correct in general terms, the answers are quantitatively different. As can be seen, the maximum effective angle at which solutions can be obtained is greater in the unsteady case by some 7%. There are differences in the two calculation procedures but it is unlikely that they are responsible for this difference. On the other hand, it is possible that the difference in the negative wall-shear values may have been influenced by the use of the FLARE approximation in the steady-state solutions. Nevertheless, the unsteady nature of the flow with $\omega = 0.001$ is clear, in spite of this very low reduced frequency.

6. Concluding remarks

The following principal conclusions may be drawn from the preceding text.

(i) A calculation method has been developed to represent flows around oscillating airfoils. It is based on a similar approach used for steady flows with separation and involves interaction between inviscid- and viscous-flow equations. The coupling technique is similar to that described by Veldman (1981) and Cebeci *et al.* (1981) for steady flows. This interactive method has been used to calculate separation and reattachment near the leading edge of a thin oscillating airfoil and has been shown to give rise to rapid convergence similar to that obtained in steady flows (Cebeci *et al.* 1986).

(ii) The accuracy of the results obtained from the solution of the boundary-layer equations has been examined with emphasis on regions of flow reversal and separation where the characteristic-box scheme is used. Attempts to improve accuracy by *ad hoc* changes to the finite-difference mesh failed and revealed the need for a procedure which would automatically guarantee accuracy by the selection of an appropriate mesh. This was achieved through a stability criterion, similar to that of Courant, Friedrichs and Lewy. The combination of this requirement and the characteristic-box scheme led to accurate solutions and showed that the mesh requirements were extremely severe in the region of large flow reversals.

(iii) Calculations have been performed for a range of reduced frequencies from 0 to 0.1. They show that increased unsteadiness allows results to be obtained at higher

angles of attack before the solutions break down; indeed in the case of the highest frequency there was no breakdown. The calculations with the standard method led to regions of flow reversal that were limited in their extent by the singularity except at the highest frequency. The interactive procedure removed this singularity and resulted in larger regions of flow reversal that involved separation at higher angles of attack.

The calculated maximum angles of attack were, however, modest and regions of separated flow were small. This is consistent with the behaviour of steady laminar flows which can only sustain small separation bubbles.

The unsteady nature of the flow at the highest frequency allowed the calculation of large regions of flow reversal and it is expected that yet higher frequencies will lead to even larger regions of flow reversal. This in turn will permit calculations to be performed at larger angles of attack where the occurrence of the singularity will require the use of the interactive procedure. The gains in angles of attack are again likely to be limited by the ability of the laminar flow to sustain separation bubbles.

(iv) The interactive scheme, incorporating the solution of the boundary-layer equations by the characteristic-box scheme and with the numerical mesh determined in accordance with the stability criterion, has been used to calculate the laminar flow for a model problem. The numerical aspects of this procedure have been thoroughly tested and shown to be general, so that it can be used for the solution of laminar and turbulent flows over airfoils of practical relevance.

This research was supported under Air Force Office of Scientific Research contract F49720-85-C-0063.

REFERENCES

CARR, L. W., MCALISTER, K. W. & MCCROSKEY, W. J. 1977 Analysis of the development of dynamic stall based on oscillating airfoil experiments. *NASA TND*-8382.

CEBECI, T. 1976 Separated flows and their representation by boundary-layer equations. *Mech. Engng Rep.* ONR-CR215-234-2. California State University, Long Beach.

CEBECI, T. 1979 The laminar boundary layer on a circular cylinder started impulsively from rest. *J. Comp. Phys.* **31**, 153–172.

CEBECI, T. 1982 Unsteady separation. In *Numerical and Physical Aspects of Aerodynamic Flows* (ed. T. Cebeci), pp. 265–277. Springer.

CEBECI, T. 1986 Unsteady boundary layers with an intelligent numerical scheme. *J. Fluid Mech.* **163**, 129–140.

CEBECI, T. & BRADSHAW, P. 1984 *Physical and Computational Aspects of Convective Heat Transfer.* Springer.

CEBECI, T. & CARR, L. W. 1981 Prediction of boundary-layer characteristics of an oscillating airfoil. In *Unsteady Turbulent Shear Flows* (ed. R. Michel, J. Cousteix and R. Houdeville), pp. 145–158. Springer.

CEBECI, T. & CLARK, R. W. 1984 An interactive approach to subsonic flows with separation. In *Numerical and Physical Aspects of Aerodynamic Flows, II* (ed. T. Cebeci), pp. 193–204. Springer.

CEBECI, T., CLARK, R. W., CHANG, K. C., HALSEY, N. D. & LEE, K. 1986 Airfoils with separation and the resulting wakes. *J. Fluid Mech.* **163**, 323–347.

CEBECI, T., KHATTAB, A. A. & SCHIMKE, S. M. 1984 Can the singularity be removed in time-dependent flows? In *Workshop on Unsteady Separated Flow* (ed. M. S. Francis and M. W. Luttges), pp. 97–105. Colorado Springs, CO.

CEBECI, T., STEWARTSON, K. & WILLIAMS, P. G. 1981 Separation and reattachment near the leading edge of a thin airfoil at incidence. *AGARD CP* 291, Paper 20.

COWLEY, S. J. 1983 Computer extension and analytic continuation of Blasius' expansion for impulsive flow past a circular cylinder. *J. Fluid Mech.* **135**, 389–405.

DALEY, D. C. & JUMPER, E. J. 1984 Experimental investigation of dynamic stall. *J. Aircraft* **21**, 831–832.

FRANCIS, M. S., KEESE, J. E. & RETELLE, J. P. 1983 An investigation of airfoil dynamic stall with large amplitude motions. *FJSRL-TR*-83-0010. F. J. Seiler Research Labs, Air Force Academy, Colorado Springs, CO.

INGHAM, D. B. 1984 Unsteady separation. *J. Comp. Phys.* **53**, 90–99.

ISAACSON, E. & KELLER, H. B. 1966 *Analysis of Numerical Methods*. Wiley.

KELLER, H. B. 1974 Accurate difference methods for two-point boundary-value problems. *SIAM J. Numer. Anal.* **11**, 305.

KELLER, H. B. 1978 Numerical methods in boundary-layer theory. *Ann. Rev. Fluid Mech.* **10**, 417–433.

KRAUSE, E., HIRSCHEL, E. H. & BOTHEMANN, TH. 1968 Die numerische Integration der Bewegungsgleichungen dreidimensionaler laminarer kompressibler Grenzschichten, Band 3. *Fachtagung Aerodynamik, Berlin.* D6LR-Fachlinchreike.

LORBER, P. F. & COVERT, E. E. 1986 Unsteady airfoil boundary layers – experiment and computation. In *Numerical and Physical Aspects of Aerodynamic Flows III* (ed. T. Cebeci), pp. 235–251. Springer.

STEWARTSON, K., SMITH, F. T. & KAUPS, K. 1982 Marginal separation. *Stud. Appl. Maths* **67**, 45–61.

VAN DOMMELEN, L. L. & SHEN, S. F. 1982 The genesis of separation. In *Numerical and Physical Aspects of Aerodynamic Flows* (ed. T. Cebeci), pp. 293–311. Springer.

VELDMAN, A. E. P. 1981 New quasi-simultaneous method to calculate interacting boundary layers. *AIAA J.* **19**, 79–85.